A NOVEL FLCBASED HYBRID ELECTRIC VEHICLE WITH MMC AND SRM DRIVE

S PAPA RAO [1]|D.KALPANA[2]|E.RAMAKRISHNA[3]
1,2 &3 Assistant Professor, EEE department, Brilliant Institute of Engineering & Technology, Hyderabad, TS.

ABSTRACT

This article examines a new fuzzy control-based hybrid electrical vehicle (HEV) that uses a modular multi-converter (MMC) to feed its switched reluctance motor (SRM). This suggested method integrates a full bridge (FB) converter with MMC fed to the SRM motor. It uses an intelligent fuzzy control algorithm to operate the FB switching pattern. The MATLAB software program has been successfully used to model the MMC inverter fed SRM drive HEvs. It is demonstrated by the simulation results that using the suggested strategy reduces the harmonics. Phase voltage, line voltage, speed, torque, rotor current, load torque, and other performance characteristics of SRM motors are measured and compared to more traditional approaches, such as solar (PV) integrated HEvs and current converter operated HEvs. obtained satisfactory output results using the suggested approach.

Keywords – MMC converter, SRM drive, BESS system

I Introduction:

Electric vehicles (EVs) and hybrid EVs (HEVs) have drawn a lot of attention due to the clean energy requirements in urban transportation. This is because of their fuel-efficient performance and environmental protection against exhaust emissions, which have been greatly supported globally [1]–[5]. HEVs have been a compromise between EVs and conventional gasoline-powered vehicles, nonetheless, given the problem of driving range anxiety and control flexibility. Permanent magnet motors are widely used in HEV power train systems because of their great efficiency and torque. However, these motors should be equipped with permanent magnets made of rare-earth elements, which are expensive and reduce the motor's performance and dependability in high-temperature and high-speed operations. Much work is being done on creating rare-earth-free motors for EVs and HEVs in order to address these drawbacks [6], [7]. Because SRMs do not include rotor windings or permanent magnets, they are known to have a more robust structure. This can result in a more affordable topology and a longer operating time under hot conditions. Additionally, its speed range is far greater than that of other motors, which is crucial for electric powertrains. Additional benefits including high torque, low complexity, high dependability, and superior fault-tolerance capability have made SRMs a viable option for powertrain systems[8]-[10].

II LITARATURE SURVEY

This paper presents the current research trends and future issues for industrial electronics related to transportation electrification. Specific emphasis is placed on electric and plug-in hybrid electric vehicles (EVs/PHEVs) and their critical drivetrain components. The paper deals with industry related EV energy storage system issues, EV charging

issues, as well as power electronics and traction motor drives issues. The importance of battery cell voltage equalization for series-connected lithium-ion (Li-ion) batteries for extended life time is presented. Furthermore, a comprehensive overview of EV/PHEV battery charger classification, standards, and requirements is presented. Several conventional EV/PHEV front-end AC/DC charger converter topologies as well as isolated DC/DC topologies are reviewed. Finally, this paper reviews various EV propulsion system architectures and efficient bidirectional DC/DC converter topologies. Novel DC/AC inverter modulation techniques for EVs are also presented. The architectures are based on the battery voltage, capacity, and driving range.

Conventional vehicles (CVs), which use petroleum as the only source of energy, represent majority of the existing worldwide on-road vehicles today. As shortage of petroleum is considered as one of the most critical worldwide issues, costly fuel becomes a major challenge for CV users. Moreover, CVs emit green house gases (GHG), thus making it harder to satisfy stringent environmental regulations. A practical and realistic solution lies in electric and plug-in hybrid electric vehicles (EVs/PHEVs). However, lithium-ion battery storage issues and charging issues have yet to be sorted out. Moreover, traction inverter and electric machine issues also need a serious thought. The bottleneck for EVs is the high voltage battery pack, which utilizes most of the space and increases the weight of the vehicle. At the same time, the large transportation sector will rely more heavily on electricity and related infrastructure needed for storage and distribution. All the above issues point towards the realization of public and private facilities to generate electricity locally, to recharge EVs and PHEVs.

This paper aims to review and present the current status and future research trends for transportation electrification from an industrial electronics standpoint. EV/PHEV charging infrastructure issues and related industrial electronics solutions are presented. The role of power electronics for onboard EV battery energy storage and management is presented. Finally, the paper reviews various EV propulsion system architectures and efficient bidirectional DC/DC converter as well as novel DC/AC traction inverter topologies.

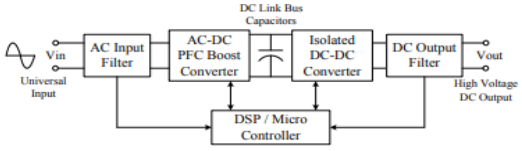

Fig. 1. Simplified system block diagram of a universal on-board two-stage battery charger.

III.PROPOSED METHOD

In the proposed MMC-based SRM drive, multiple working modes are achieved, including the battery driving mode, generator control unit (GCU) driving mode, GCU-battery driving mode, running charging mode, standstill charging mode, and battery fault-tolerance mode. The advantages of the proposed topology are: 1) multiple working modes can be flexibly selected by controlling the MMC and full-bridge converter; 2) the MMC-based topology can drive the SRM from variable dc voltages according to the running speed to reduce the voltage stress on the switches which also improves the reliability; 3) multilevel phase voltage is achieved due to additional battery charging in running conditions, which improves the

torque capability; 4) by using standard half-bridge modules for both the MMC and full-bridge converter, completely modular topology is achieved; 5) flexible charging functions can be directly achieved through the proposed drive without external ones, including the running charging and standstill charging modes; 6) flexible fault-tolerance ability for each battery cell is equipped by easily bypassing the faulty one; 7) the battery state-of-charge (SOC) can be balanced by controlling the sub module charging according to the SOC level.

3.1 CONVENTIONAL SRMDRIVES

Fig. 3.1 illustrates the diagram of a three-phase 12/8 SRM drive, mainly including a power converter, an SRM, a drive circuit, current sensors, a position sensor, and a current controller. Phase currents are detected by individual current sensors for the implementation of the current control strategy. Considering the phase isolation characteristic and excellent fault-tolerance capability, the asymmetrical half-bridge converter is usually employed for the SRM drive, where each phase leg can be independently controlled by two switching devices. For the current controller, hysteresis control method is usually used. The hysteresis control system is a nonlinear system, which has excellent loop performance, global stability, and small phase lag. Therefore, the current hysteresis control is inherently stable and robust to dynamic perturbations, and the system is more stable and has fast dynamic response due to its inherent non-linearity.

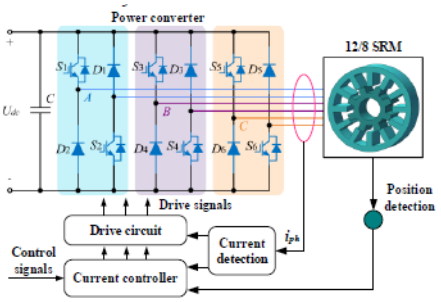

Fig. 3.1. Diagram of the three-phase 12/8 SRM drive.

Fig. 2 shows the three switching modes of phase A in the asymmetrical half-bridge converter, including the excitation mode, freewheeling mode, and demagnetization mode. When switches S1 and S2 are both turned on, the dc power source supplies the current to the phase A winding, and this phase works in the excitation mode (see Fig. 2(a)), where the phase voltage is positive dc bus voltage Udc; when the switch S1 is turned off and S2 is still on, the phase A current flows through S2 and diode D2 in a zero-voltage loop (ZVL), where phase A is in the ZVL mode (see Fig. 2(b)); when switches S1 and S2 are both turned off, the phase A current flows back to the dc source through diodes D1 and D2, and phase A is in the demagnetization mode (see Fig. 2(c)), where the phase voltage is negative dc bus voltage -Udc.

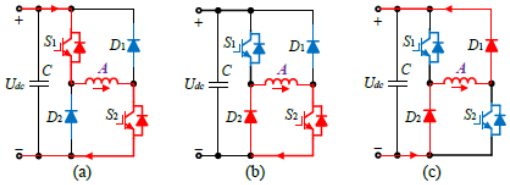

Fig.3.2. Switching modes of the asymmetrical half-bridge converter. (a) Excitation mode. (b) ZVL mode. (c) Demagnetization mode.

The voltage equation for each phase can be expressed in terms of the current, inductance, and rotor position as

$$U_k = R_k i_k + L_k(\theta, i_k)\frac{di_k}{dt} + \frac{\partial L_k(\theta, i_k)}{\partial \theta}\omega i_k \qquad (1)$$

where Uk is the phase voltage, Rk is the phase winding resistance, ik is the phase current, θ is the rotor position, Lk is the phase winding inductance which varies as a function of the rotor position, ω is the rotor angular speed, and k=a, b, c phase. The output torque of the three-phase SRM is the sum of individual phase torques, which is expressed as

$$T_e = \sum_{k=1}^{3} T_{ek} = \sum_{k=1}^{3} \frac{1}{2} i_k{}^2 \frac{\partial L_k(i_k,\theta)}{d\theta} \qquad (2)$$

When a current is applied in the inductance ascending region, a positive phase torque can be obtained; while applying a current to a phase winding in the inductance descending region leads to a negative phase torque. The mechanical equation of the SRM is expressed as

$$J\frac{d\omega}{dt} + \mu\omega = T_e - T_l \qquad (3)$$

Where Te is the output torque, Tl is the load torque, J is the combined moment of inertia of the motor and load, and μ is the combined friction coefficient of the motor and load. However, for conventional SRM drives, the dc bus voltage is fixed and the voltage stress on switches cannot be reduced by changing the dc bus voltage according to the running speed. The multilevel phase voltage cannot be achieved which limits the output torque in high-speed operations. Also, the fault tolerance for battery cells and flexible charging functions are not achieved. This paper proposes a MMC-based SRM drive with decentralized battery energy storage system (BESS) for HEVs. Compared to conventional and existing SRM drives, the presented topology has several advantages, including flexible dc bus voltage, multilevel phase voltage, and modular structure, fault-tolerance ability for battery cells, flexible running charging, grid-connecting charging, and SOC balancing capability, which will be analyzed in detail in followings.

3.2. Proposed MMC-Based SRM Drive

Fig. 3 shows the developed MMC with decentralized BESS. A half-bridge converter and a battery pack Ex are employed as a sub module (SM), and each SM is made up of two insulated-gate bipolar transistors (IGBTs), including a upper switch Sx1 and a lower switch Sx2. The output voltage of each SM is Usm, which is determined by the SM working state according to the on-off state of two switches, and multiple SMs are connected in series to form a decentralized BESS for the total dc bus voltage Udc. In this configuration, battery cells are decentralized by individual SMs, and each battery cell SM can be controlled independently.

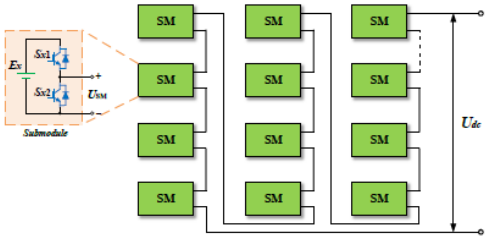

Fig. 3.3. Developed MMC with decentralized BESS.

As shown in Fig. 3.4, each SM is a two-level half-bridge converter consisting of a battery cell and two switches. In the IGBT, there is an integrated antiparallel diode. The state of the antiparallel diode is defined as on when there is a current flowing through it, and defined as off with no current. The operation states of the two-level SM under different IGBT switching states are presented in Fig. 3.4 and Table I.

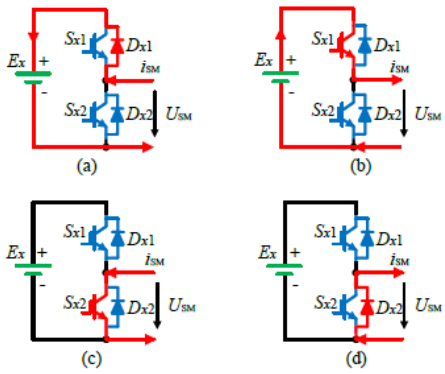

Fig. 3..4. Operation states of a two-level SM. (a) Discharging mode. (b) Charging mode. (c) Bypass mode 1. (d) Bypass mode 2.

SM OPERATION STATES

SM state	S_{x1}	S_{x2}	D_{x1}	D_{x2}	U_{sm}	i_{sm}	E_x
On	On	Off	Off	Off	U_{by}	Positive	Discharging mode
On	Off	Off	On	Off	$-U_{by}$	Negative	Charging mode
Off	Off	On	Off	Off	0	Negative	Bypass mode
Off	Off	Off	Off	On	0	Positive	Bypass mode

TABLE I

$$U_{sm}=\begin{cases}U_{by}, & S_{x1}\ is\ on,\ S_{x2}\ is\ off,\ D_{x1}\ is\ off,\ D_{x2}\ is\ off\\ -U_{by}, & S_{x1}\ is\ off,\ S_{x2}\ is\ off,\ D_{x1}\ is\ on,\ D_{x2}\ is\ off\\ 0, & S_{x1}\ is\ off,\ S_{x2}\ is\ on,\ D_{x1}\ is\ off,\ D_{x2}\ is\ off\\ 0, & S_{x1}\ is\ off,\ S_{x2}\ is\ off,\ D_{x1}\ is\ off,\ D_{x2}\ is\ on\end{cases} \quad (4)$$

The dc bus voltage is the sum of the SM output voltages, given by

$$U_{dc}=NU_{sm} \quad (5)$$

Where N is number of total SMs.

In order to illustrate the functions of the proposed drive more clearly, a simplified system with six SMs is adopted as an example in this paper for analysis. Fig. 5 shows a MMC-based SRM drive with six SMs for HEV applications, including a MMC-based decentralized BESS and a modular full-bridge converter. The full-bridge converter is used to achieve a completely modular converter structure, where the commercial power modules can be directly used for the proposed drive, which is beneficial for the market mass production [42]-[44]. Furthermore, the full-bridge converter can also provide a flexible fault-tolerant operation for power switch faults with bipolar excitation [42], [43], which is suitable for high-performance and safety-critical vehicle applications. The MMC is composed of six SMs by using IGBTs with integrated fast recovery antiparallel diode, an energy storage unit including five battery packs (E1~E5), and a GCU including a generator (G), a relay (J), a rectifier (RE), and a capacitor (C). In the modular full-bridge converter, six half-bridge modules are used to drive the three-phase SRM, where two half-bridge modules are employed for one phase, which achieves a completely modular structure for massive production. By employing the proposed SRM drive, multiple working modes can be flexibly achieved and the system performance can be improved.

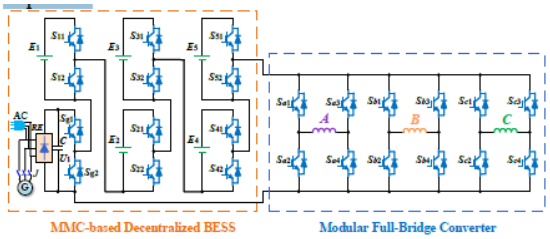

Fig. 3.5. MMC-based SRM drive with six SMs for HEVs.

A battery energy storage system for EVs is composed of several battery packs connected in series to satisfy a voltage and capacity specification [45], [46]. Therefore, each battery pack can be easily connected with a converter for independent control [47], [48]. For MMC topologies, the battery packs can be connected with MMC submodules for conventional AC motor drives in EVs [39], [49], [50], allowing high flexibility for the discharge and charge of each battery pack. In these papers, to reduce the complexity of the converter circuit for analysis, four to six submodules are usually adopted for phase for the proof of concept. Therefore,

in this paper, in order to explain the principle of the proposed SRM drive more clearly with reduced complexity, six submodules connecting with five battery packs and a GCU are just adopted for analysis and experiments. However, MMCs show excellent expansibility [39], [49], [50]. Hence, more flexible dc bus voltage, multilevel voltage, battery discharging and charging, and battery fault tolerance ability can be further achieved by employing more battery submodules for the proposed SRM system.

3.3. Battery Driving Mode

3.3.1) Full Battery Cells Driving When the relay J is off and switch Sg2 is on, the GCU SM is bypassed and the proposed SRM drive can work in pure-battery driving mode. In this condition, the dc bus voltage can be flexibly controlled by employing different SMs. Fig. 6 presents the working stages of the motor drive in battery driving mode with flexible excitation and demagnetization voltages. Fig. 6(a) shows the condition that E1~ E5 are all employed for excitation, where switches S11, S21, S31, S41, and S51 are all turned on, and S12, S22, S32, S42, and S52 are all kept off for the phase winding excitation; in the winding demagnetization mode, the current flows back to the power source through S11, S21, S31, S41, and S51, as shown in Fig. 6(b). For this condition, the discharging and charging voltage for the dc link is given by

$$U_{dc}=\begin{cases}5U_{sm}, & Discharging\ state\\ 5U_{sm}, & Charging\ state\end{cases}$$

The phase A voltage is directly the dc bus voltage in this condition, which can be expressed as

$$U_a=\begin{cases}5U_{sm}, & Phase\ A\ excitation\\ -5U_{sm}, & Phase\ A\ demagnetization\end{cases} \quad (7)$$

3.3.2) Two Battery Cells Driving with Two Additional Battery Cells Charging

Fig. 3.6(c) and (d) present the conditions that two battery cells are employed for the winding excitation, and additional two SMs are employed to improve the voltage for winding demagnetization and achieve battery charging during running conditions. For example, E1 and E2 are used to supply the power to the motor, and E3 and E4 are employed to increase the demagnetization voltage, where S11 and S21 are both turned on, and S52 are also turned on to bypass the E5 SM. In the excitation mode of phase A, the current flows through S11 and S21, the diodes in S32 and S42, and the bypass switch S52 to phase A converter, as shown in Fig. 6(c); when phase A is turned off, the demagnetization current goes through the bypass switch S52, the diodes in S31 and S41, and switches S11 and S21 to the power source, as shown in Fig. 3.6(d). The demagnetization voltage is elevated by E3 and E4, where the multilevel phase voltage can be achieved to accelerate both the excitation and demagnetization processes for torque improvements, and also E3 and E4 can be charged by the demagnetization current. In this condition, the charging and discharging voltage for the dc link is given by

$$U_{dc}=\begin{cases}2U_{sm}, & Discharging\ state\\ 4U_{sm}, & Charging\ state\end{cases} \quad (8)$$

The phase A demagnetization voltage is directly increased to -4Usm due to additional battery cells charging. Although the dc bus voltage is only 2Usm in the discharging mode, the excitation

voltage of phase A can still be elevated to 4Usm by phase C demagnetization, according to the current overlapping states [24], [29]. When phase C current is larger than phase A current in the phase C demagnetization stage, phase C winding works as a current source to supply the current to phase A and simultaneously charge the battery. Because the phase C winding is under the demagnetization voltage -4Usm due to the battery cell E3 and E4 charging, the phase A voltage can be elevated to 4Usm when phase C winding supplies the current to phase A. When phase C current decreases to be smaller than phase A current, the dc-link power source and phase C both supply the current to phase A, and the phase A voltage returns to 2Usm. Hence, after the excitation current quickly established at the beginning of the turn-on region with an increased voltage, the phase voltage can immediately decrease to the power supply voltage in the main turn-on region, which not only improves the torque, but also achieves a lower excitation voltage.

Therefore, multilevel phase voltage is achieved in the proposed drive and the phase A voltage can be expressed as

$$U_a=\begin{cases}4U_{sm}, & \text{Phase A excitation, Phase C demagnetization, } i_c>i_a\\ 2U_{sm}, & \text{Phase A excitation, Phase C demagnetization, } i_c<i_a\\ -4U_{sm}, & \text{Phase A demagnetization, Phase B excitation, } i_a>i_b\\ -2U_{sm}, & \text{Phase A demagnetization, Phase B excitation, } i_a<i_b\\ -4U_{sm}, & \text{Phase A demagnetization, Phase B in ZVL, } i_a<i_b\end{cases}$$ (

3.3.3) One Battery Cell Driving with Two Additional Battery Cells Charging

Fig. 6(e) and (f) illustrate that only E1 is employed to supply the power, and E2 and E5 are used for charging, where S11 is turned on, and S32 and S42 are also turned on to bypass E3 and E4. When phase A is in the turn-on region, E1 provides the current flowing through the switch S11, the diodes of S22 and S52, and switches S32 and S42, as shown in Fig. 6(e); when phase A is turned off, the current goes back to the power supply through S42 and S32, the diodes of S51 and S21, and the switch S11, as shown in Fig, 6(f). In this condition, E2 and E5 are employed to additionally increase the demagnetization voltage, which are also charged by the demagnetization current. The discharging and charging voltage for the dc link in this condition is given by

$$U_{dc}=\begin{cases}U_{sm}, & \text{Discharging state}\\ 3U_{sm}, & \text{Charging state}\end{cases}\qquad(10)$$

Similarly, the phase A voltage can be expressed as follow

$$U_a=\begin{cases}3U_{sm}, & \text{Phase A excitation, Phase C demagnetization, } i_c>i_a\\ U_{sm}, & \text{Phase A excitation, Phase C demagnetization, } i_c<i_a\\ -3U_{sm}, & \text{Phase A demagnetization, Phase B excitation, } i_a>i_b\\ -U_{sm}, & \text{Phase A demagnetization, Phase B excitation, } i_a<i_b\\ -3U_{sm}, & \text{Phase A demagnetization, Phase B in ZVL, } i_a<i_b\end{cases}\qquad(11)$$

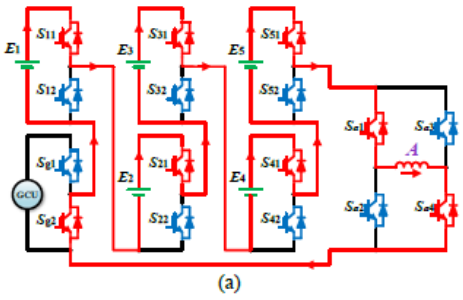

(a)

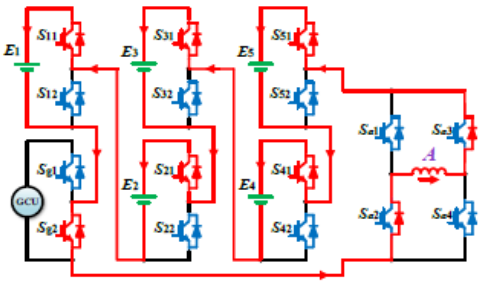

(b)

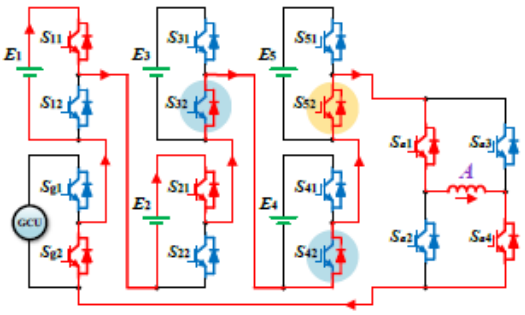

(c)

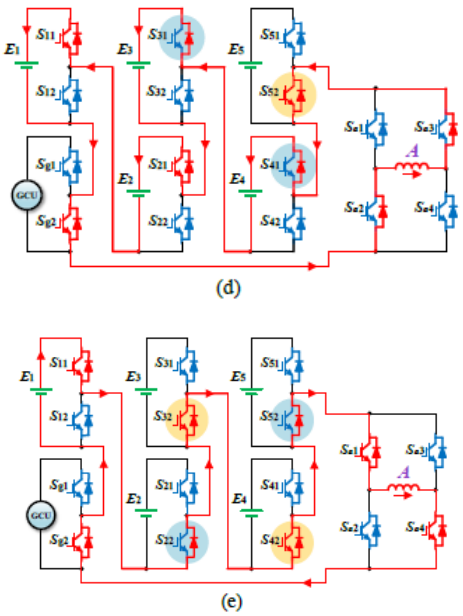

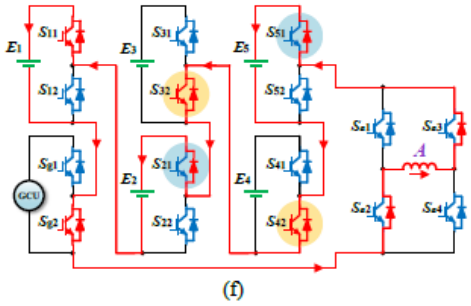

Fig.3.6. Battery driving mode by employing different SMs. (a) E1~E5 are all employed for excitation. (b) E1~ E5 are all employed for demagnetization. (c) E1 and E2 are employed for excitation. (d) E1, E2, E3, and E4 are employed for demagnetization. (e) E1 is employed for excitation. (f) E1, E2, and E5 are employed for demagnetization.

IV Simulation Results:

In below figure.3 proposed simulation results Ia, Ib and Ic are represents the phase currents Va, Vb and Vc are phase voltages for better understanding only Vb phase is highlated. Iby reprents the battery current.

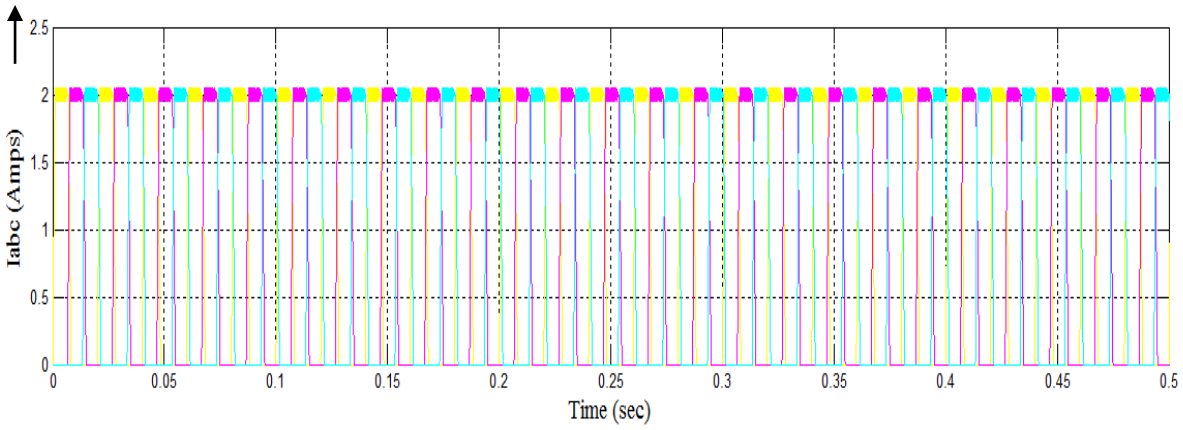

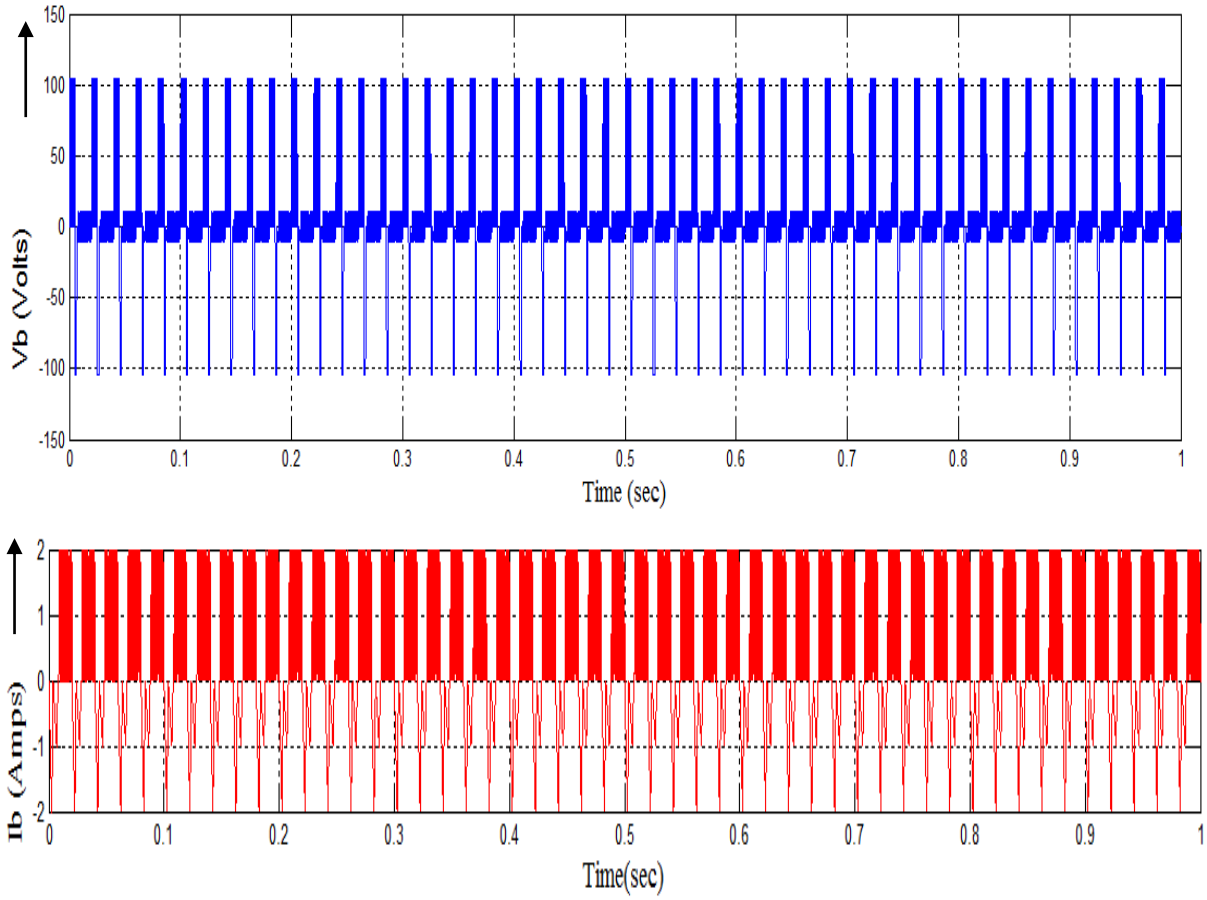

Fig.17 (a, b, & c) Performance of battery driving at full voltage

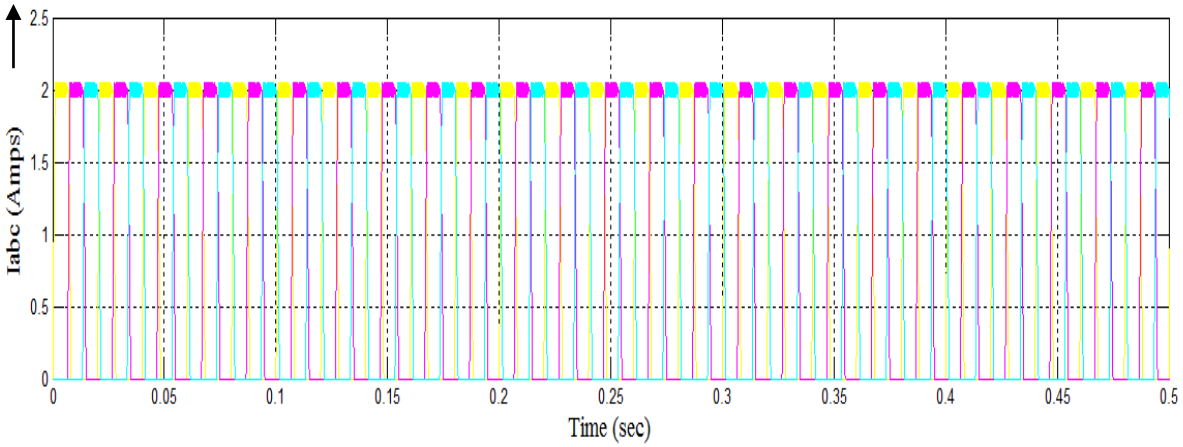

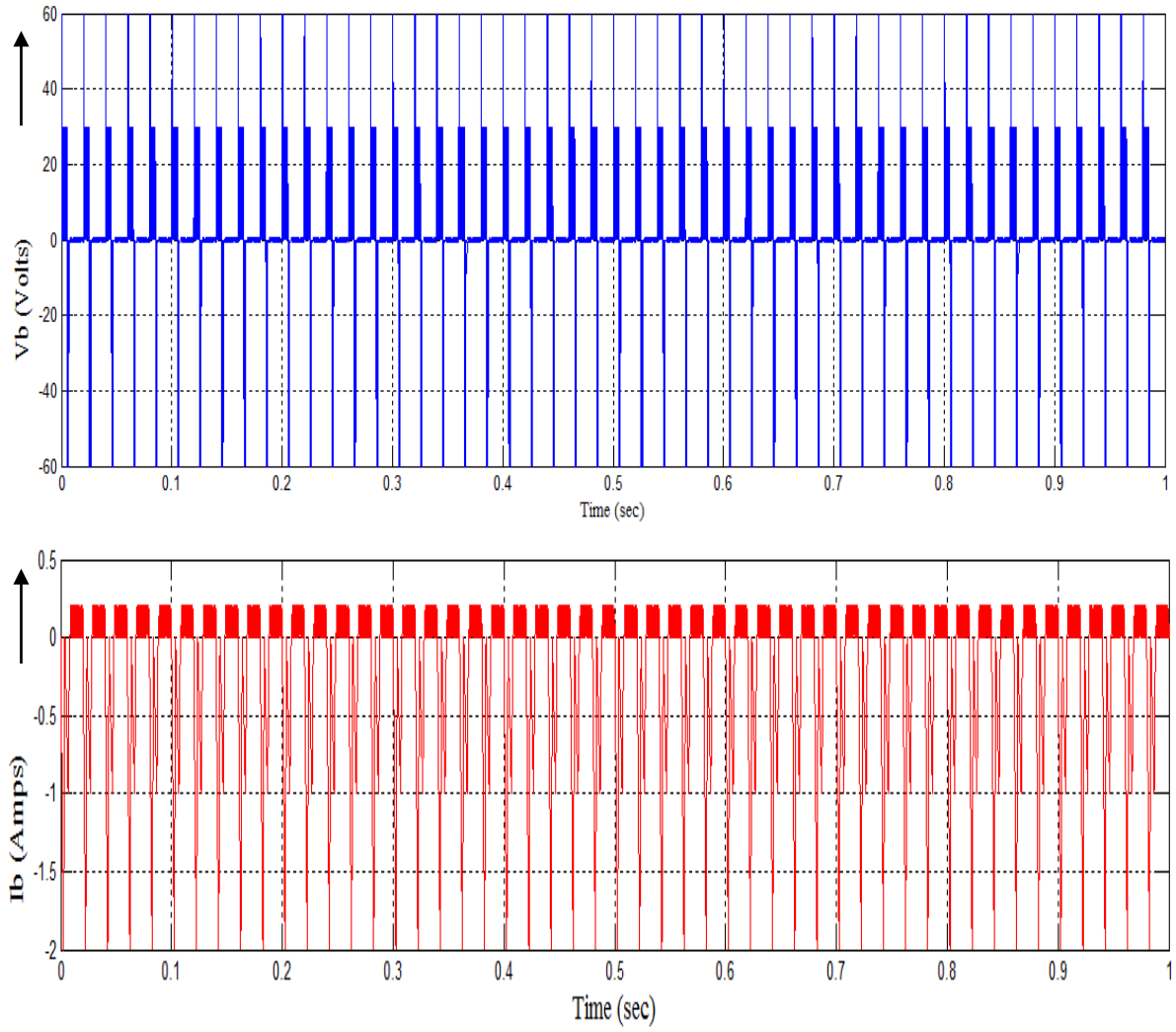

Fig.3(a, b, & c) Performance of battery driving with E1 and E2 with E3 and E4 charging

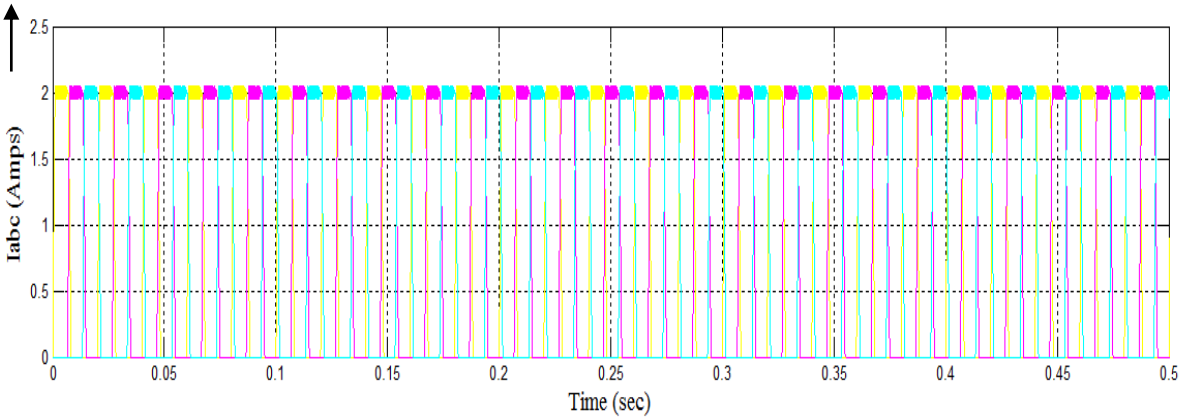

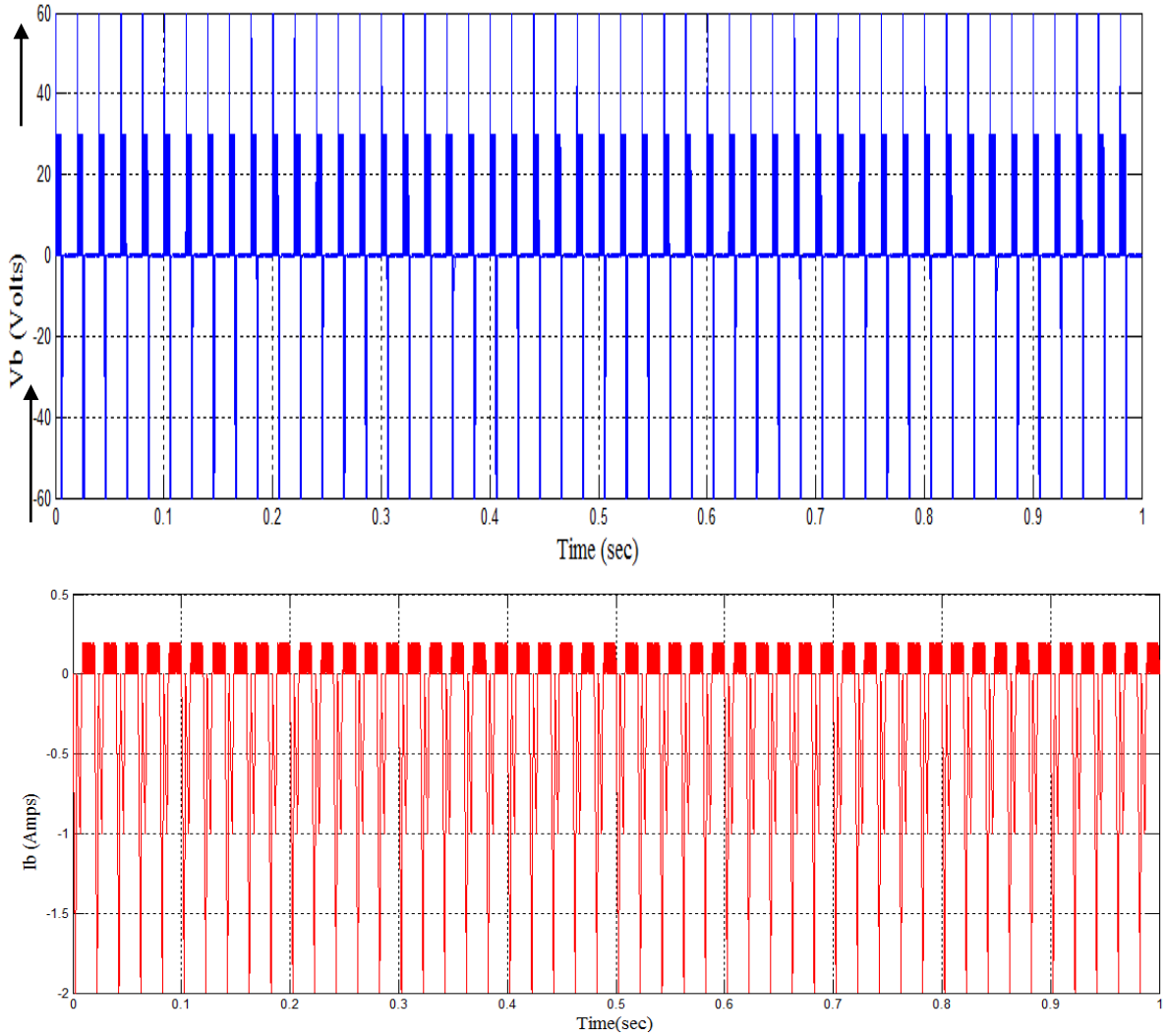

Fig.4(a, b, & c) Performance of battery driving with E1 with E2 and E5 charging

V CONCLUSION

This study discusses the design of HEVs using an MMC-based SRM motor. Using the SRM motor fuzzy control method improves the SRM motor's dynamic responsiveness. obtained simulated results for HEV charging and discharging modes in the suggested way and shown its effectiveness in comparison to other conventional methods. It is noted that the load torque varies when the input step speed varies at constant current, and it is stated how the load torque varies when the phase current varies at constant speed. It is clear from the suggested simulation results that there is a significant reduction in output voltage harmonics. The simulation of the SRM motor based on an MMC converter has been accomplished. By connecting the phases to a number of batteries, the MMC converters provide different voltage levels.

REFERENCES

[1] S. S. Williamson, A. K. Rathore, and F. Musavi, “Industrial electronics for electric transportation: current state-of-the-art and future challenges,” IEEE Trans. Ind. Electron. vol. 62, no. 5, pp. 3021-3032, May 2015.

[2] A. A. Ferreira, J. A. Pomilio, G. Spiazzi, and L. de Araujo Silva, “Energy management fuzzy logic supervisory for electric vehicle power supplies system,” IEEE Trans. Power Electron., vol. 23, no. 1, pp. 107-115, Jan. 2008.

[3] G. Carli and S. S. Williamson, "Technical considerations on power conversion for electric and plug-in hybrid electric vehicle battery charging in photovoltaic installations," IEEE Trans. Power Electron., vol. 28, no. 12, pp. 5784-5792, Dec. 2013.

[4] O. C. Onar, J. Kobayashi, and A. Khaligh, "A fully directional universal power electronic interface for EV, HEV, and PHEV applications," IEEE Trans. Power Electron., vol. 28, no. 12, pp. 5489-5498, Dec. 2013.

[5] A. Emadi, Y. J. Lee, and K. Rajashekara, "Power electronics and motor drives in electric, hybrid electric, and plug-in hybrid electric vehicles," IEEE Trans. Ind. Electron., vol. 55, no. 6, pp. 2237–2245, Jun. 2008.

[6] Z. Yang, F. Shang, I. P. Brown, and M. Krishnamurthy, "Comparative study of interior permanent magnet, induction, and switched reluctance motor drives for EV and HEV applications," IEEE Trans. Transport. Electrific., vol. 1, no. 3, pp. 245-254, Oct. 2015.

[7] I. Boldea, L. N. Tutelea, L. Parsa, and D. Dorrell, "Automotive electric propulsion systems with reduced or no permanent magnets: an overview," IEEE Trans. Ind. Electron., vol. 61, no. 10, pp. 5696-5711, Oct. 2014.

[8] M. Krishnamurthy, C. S. Edrington, A. Emadi, P. Asadi, M. Ehsani, and B. Fahimi, "Making the case for applications of switched reluctance motor technology in automotive products," IEEE Trans. Power Electron., vol. 21, no. 3, pp. 659-675, May 2006.

[9] E. Bostanci, M. Moallem, A. Parsapour, and B. Fahimi, "Opportunities and challenges of switched reluctance motor drives for electric propulsion: a comparative study," IEEE Trans. Transport. Electrific., vol. 3, no. 1, pp. 58-75, Mar. 2017.

[10] J. Cai and Z. Deng, "Unbalanced phase inductance adaptable rotor position sensorless scheme for switched reluctance motor," IEEE Trans. Power Electron., vol. 33, no. 5, pp. 4285-4292, May 2018.